Journal of Medicinal Chemistry

ARTICLE

pubs.acs.org/jmc

Inhibition of Cell Proliferation by Quindoline Derivative (SYUIQ-05) through its Preferential Interaction with *c-myc* Promoter G-Quadruplex

Tian-Miao Ou,[†,§] Jing Lin,[†,§] Yu-Jing Lu,[‡] Jin-Qiang Hou,[†] Jia-Heng Tan,[†] Shu-Han Chen,[†] Zeng Li,[†] Yan-Ping Li,[†] Ding Li,[†] Lian-Quan Gu,[*,†] and Zhi-Shu Huang[*,†]

[†]School of Pharmaceutical Sciences, Sun Yat-sen University, Guangzhou University City, Waihuan East Road 132, Guangzhou 510006, People's Republic of China

[‡]Faculty of Chemical Engineering and Light Industry, Guangdong University of Technology, Guangzhou 510006, People's Republic of China

Supporting Information

ABSTRACT:

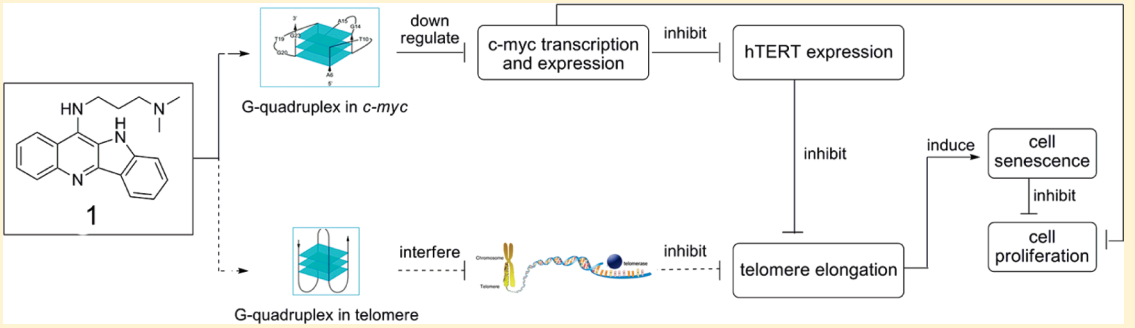

G-Quadruplex is a special DNA secondary structure and present in many important regulatory regions in human genome, such as the telomeric end and the promoters of some oncogenes. Specially, different forms of G-quadruplexes exist in telomeric DNA and *c-myc* promoter and play important roles in the pathway of cell proliferation and senescence. The effects of G-quadruplex ligands for either telomeric or *c-myc* G-quadruplex in vitro have been widely studied, but the specificity of these effects in vivo is still unknown. In the present research, various experiments were carried out to study the effect of G-quadruplex ligand SYUIQ-05 on tumor cell lines and the mechanism of this effect. Our results showed that it preferred to bind with G-quadruplex in *c-myc* and had rather insignificant effect on G-quadruplex in telomere. Therefore, it is possible that this compound had its antitumor activity for cancer cells mainly through its interaction with *c-myc* quadruplex.

INTRODUCTION

Guanine-rich (G-rich) stretches of DNA have a high propensity to self-associate into planar guanine quartets (G-quartets) that assembled to give unusual structures called G-quadruplexes. Quadruplexes are present in many important regulatory regions in human genome, including telomeric ends, immunoglobulin switch regions, mutational hot spots, and regulatory elements in oncogene promoters.[1] The formation or stabilization of G-quadruplexes in these regions may play an important regulatory role, and therefore G-quadruplexes are recognized as promising targets for the design of antitumor drugs.[2−4]

Many different structural G-quadruplex ligands display their various effects on tumor cells including telomerase inhibition,[2] telomere shortening,[5] triggering cell growth arrest,[6−8] inducing autophagy and apoptosis,[9−11] end-to-end fusion associated with the appearance of p16-associated senescence,[12] and down-regulating the transcription or expression of related gene.[13,14] As for the studies on *c-myc* G-quadruplex, the porphyrin derivatives TMPyP4, TMPyP2, and Se2SAP are the first identified class of *c-myc* G-quadruplex ligands.[15,16]

Because of the complicated network of various genes in vivo, it is hard to explain clearly their real effects on quadrome genes in tumor cells. For example, G-rich sequences in the promoter of oncogene *c-myc* can form G-quadruplexes and regulate the transcription of oncogene *c-myc*. In addition, this *c-myc* gene encodes the important transcriptional regulation protein c-Myc that controls a variety of other genes responsible for enhancing the proliferative capacity of cells.[17] Especially, c-Myc transcriptionally activates hTERT, the catalytic subunit of telomerase,[18] and consequently influences the elongation of telomere, which is another important quadrome gene involved in cell senescence.[19]

Received: January 20, 2011
Published: July 20, 2011

dx.doi.org/10.1021/jm200062u | *J. Med. Chem.* 2011, 54, 5671–5679

It is important to know whether the G-quadruplex ligand can specifically bind to one or a few targets in tumor cells, which will be helpful for the discovery of selective G-quadruplex interactive agents.

Quindoline is one type of alkaloid natural product, and some derivatives of it are found to be G-quadruplex ligands.[13,20−22] The quindoline derivative **1**, *N*′-(10*H*-indolo[3,2-*b*]-quinolin-11-yl)- *N*,*N*-dimethyl-ethane-1,2-diamine (SYUIQ-05), is found to interact with human telomere or *c-myc* oncogene and has effects on the biological functions of these two genes, resulting in telomere shortening, autophagy, inhibition of cell proliferation, cell senescence, and apoptosis.[13,20,22] As we can see from the above references, **1** is identified as G-quadruplex ligand for both telomere and *c-myc*, while whether it has a selectivity between these two quadruplex DNAs is still unknown. Some of our previous studies showed that the interaction ability of **1** on telomeric quadruplex is not as strong as that on *c-myc* quadruplex (data not published). Because of the importance of finding the real selective ability of ligands in tumor cells, we tried to reveal this effect of **1** in the present study by comparing its in vitro interaction on telomeric quadruplex and *c-myc* quadruplex in parallell, and more importantly, we tried to compare its effects on cellular events relating to c-Myc or telomere and find out the promising connection between the in vitro selectivity and the in vivo events. The major mechanisms for the antitumor activity of **1** were proposed and discussed based on multiple in vitro and in vivo experiments. Briefly, **1** was found to bind preferentially with G-quadruplex in *c-myc* with rather insignificant effect to G-quadruplex in telomere based on the results of in vitro assays. Consistently, it was also found that **1** exhibited its antitumor activity for tumor cells mainly due to its interaction with *c-myc* based on the results of in vivo assays.

RESULTS

The Compound Preferred to Bind to G-Quadruplex in *c-myc* in Vitro. The binding affinity of **1** with two G-quadruplex DNA, the telomeric G-rich DNA (HTG21), and the G-rich sequence in the promoter of *c-myc* (Pu27) were studied using FRET-melting, PCR stop assay, ITC, and MD, the docking picture are shown in Supporting Information Figure S1, and the raw data of FRET-melting, PCR stop assay, and ITC are shown in Supporting Information Figures S2, S3, and S4, respectively. In solution containing potassium ions, the HTG21 DNA preferred to fold into an intramolecular hybrid G-quadruplex, while the Pu27 DNA preferred to form a parallel conformation. The calculated or measured binding affinity for **1** with two G-quadruplex DNA were listed in Table 1, showing the changes in binding free energy (ΔG), the changes in melting temperature of G-quadruplex DNA (ΔT_m), the concentrations for 50% inhibition in DNA amplification (IC_{50}), and the binding constant (K_a). The data from different methods showed good correlation with each other, indicating the binding of the ligand with G-quadruplex DNA might increase its stability resulting in interference with its DNA amplification. All the in vitro experimental data indicated that **1** preferred to bind with the G-quadruplex in the promoter region of *c-myc*, showing a relatively higher thermodynamic stability, stronger inhibitory activity on the hybridization of G-rich sequence with its complementary strand, higher binding constant, and lower free energy.

Down-Regulation of the Transcription and Expression of *c-myc* and Thus hTERT by the Compound. Oncogene *c-myc* encodes an important transcriptional regulator c-Myc protein, which is involved in cell proliferation, senescence, and apoptosis.[23] Meanwhile, human telomerase reverse transcriptase (hTERT) is the key catalytic domain of the telomerase enzyme, which is closely related to telomerase function and regulated by c-Myc protein.[24] Because *c-myc* promoter region contains G-quadruplex forming G-rich sequence, its binding with **1** should increase its stability resulting in down-regulation of *c-myc* transcription and its further downstream gene *hTERT*, which would be identified using real-time RT-PCR.

Table 1. Binding Affinity of 1 with Two G-Quadruplex DNA

DNA	ΔG[a]	ΔT_m,[b] °C	IC_{50},[c] μmol/L	K_a,[d] mol/L
HTG21	−22.16	10	2.5	$(1.79 \pm 0.68) \times 10^4$
Pu27	−29.82	13	1.8	$(4.03 \pm 0.34) \times 10^4$

[a] Estimated binding free energy calculated by MM-PBSA. The figure of models is shown in Supporting Information Figure S1. [b] Changes of melting temperatures were calculated from FRET-melting assay data. The raw FRET-melting assay data are shown in Supporting Information Figure S2. [c] Concentrations for 50% inhibition were calculated from PCR stop assay data. The gel pictures are shown in Supporting Information Figure S3. [d] Binding constants were obtained from the ITC measurement. The figure of original ITC titration data is shown in Supporting Information Figure S4.

To test the above hypothesis and understand the effect of **1** on *c-myc*, two Burkitt's lymphoma cell lines with different translocation break points within the *c-myc* were tested. The Ramos cell line retains the NHE III_1 during translocation, while the CA46 cell line has this element removed together with the P1 and P2 promoters[23,25] and therefore cannot form the G-quadruplex structure. First, cellular uptake experiment was taken to confirm that the transport efficiency of **1** in Ramos cell was similar to that in CA46 cell (data shown in Supporting Informaiton Figure S5). On the basis of this result, further studies were carried out in these two cells, including real-time RT-PCR (raw data are shown in Supporting Information Table S1 and S2) and Western Blot assay. As shown in Figure 1A, **1** could down-regulate the transcription of *c-myc*, which further down-regulate its regulation gene *hTERT* in Ramos cells, while this inhibitory activity on the transcription was not found in CA46 cells. This result indicated that the down-regulation effect of **1** on these two genes might be mainly due to its interaction with the G-quadruplex in the promoter of *c-myc*.

Western Blot was also carried out to confirm the inhibitory activity of **1** on the expression of these two genes. The result was shown in Figure 1B, which demonstrated that **1** could inhibit the expression of c-Myc and hTERT in Ramos cell. On the other hand, **1** could inhibit the expression of c-Myc in CA46 cell, while the effect of it on hTERT still needs further evidence because the expression level of hTERT in CA46 cell was too low to detect.

The Compound Interfered with the Interaction between G-Quadruplex DNA and its Binding Proteins. NM23-H2 is an important transcription regulation protein, which is capable of activating *c-myc* transcription via the NHE III_1 region.[24] Importantly, the stabilization of the G-quadruplex structures within the NHE III_1 region blocks the recognition and remodeling functions of NM23-H2.[26,27] Here chromatin immunoprecipitation (ChIP) was used to probe physical occupancy of NM23-H2 to *c-myc* promoter in human cervical epithelial carcinoma cell HeLa S3. Rabbit polyclonal-nm23-H-antibody was used for ChIP to retrieve DNA sequences bound to endogenous NM23-H2. PCR

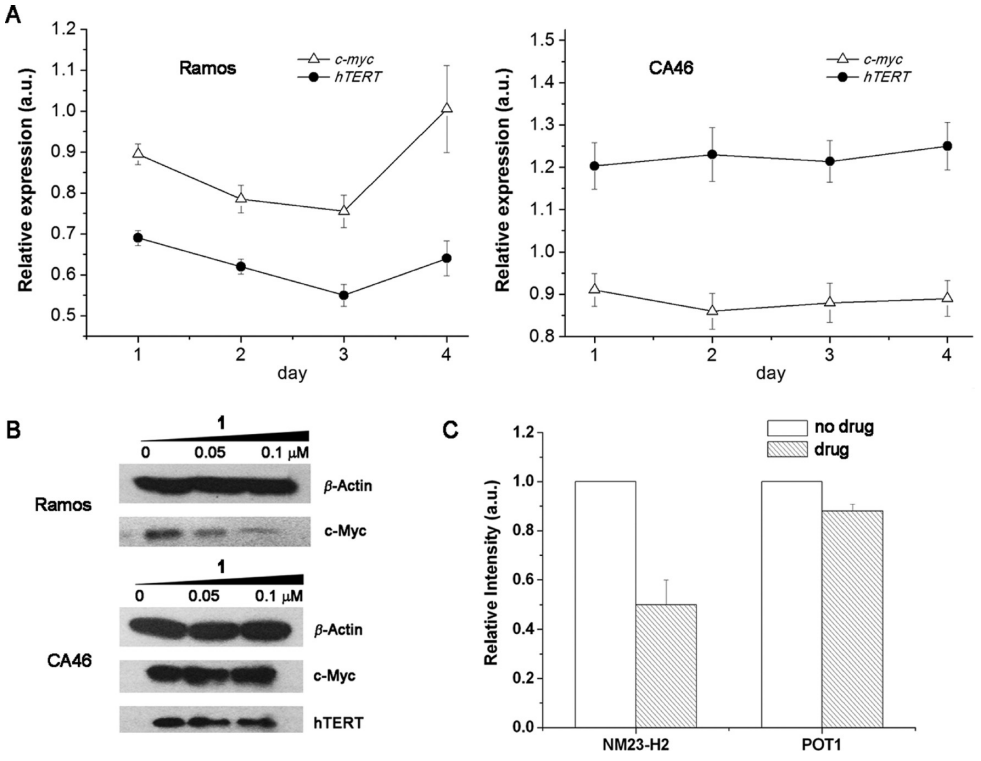

Figure 1. (A) qRT-PCR to determine the transcription of *c-myc* and *hTERT* in the Ramos (left) and CA46 (right) cells treated with **1**. The cells were treated with medium or 0.1 μM of **1** for 4 days, and the total RNA was extracted every day and subjected to reverse transcription, followed with qPCR for *c-myc*, *hTERT*, and β-actin (internal control), whose data are shown in Supporting Information Table S1 and S2. The quantity of gene expression was calculated with ct values and plotted in graph. (B) Western Blot was used to determine the expression of *c-myc* and hTERT in the Ramos (upper) and CA46 cells treated with **1**. The cells were treated with medium and 0.05 or 0.1 μM of **1** for 4 days, and the total protein was extracted every day and subjected to Western Blot for *c-myc*, hTERT, and β-actin (internal control). The photo of hTERT in CA46 was not shown because the expression level of hTERT in CA46 was too low to detect. (C) ChIP assays were carried out using antibodies against NM23-H2 or POT-1 in HeLa cells treated with 0.1 μM **1** or 0.1% DMSO as negative control, respectively. Immunoprecipitated DNA samples were amplified with qPCR to show NM23-H2 occupancy of *c-myc* promoter or POT-1 occupancy of telomeric single-stranded end and negative controls. The qPCR data are shown in Supporting Information Table S3.

amplification of *c-myc* promoter showed significant decrease in immunoprecipitated samples after the treatment with **1** (Figure 1C, and the raw qPCR data are shown in Supporting Information Table S3). This result indicated that **1** could interfere with the binding between the promoter region of *c-myc* and NM23-H2, which might contribute to its inhibitory activity on the transcription of *c-myc*.

To further study the dissociation effect of **1** on the binding between *c-myc* promoter and NM23-H2, we cotransfected an EGFP-NM23-H2 fusion plasmid and a luciferase plasmid carrying the wild-type promoter region of *c-myc* into a HeLa cell. After DAPI staining and imaged using a laser scanning confocal microscope (Figure 2), the dissociation of NM23-H2 and *c-myc* was clearly observed in the transfected cells after the treating with **1**. While after cotransfecting an EGFP-NM23-H2 fusion plasmid and a luciferase plasmid carring the mutant promoter region of *c-myc*, which could not form G-quadruplex again,[26] the incubation of **1** could not dissociate the binding of NM23-H2 and *c-myc*. These results strongly supported that the compound could induce the forming of G-quadruplex and thus dissociate the binding of NM23-H2 and the promoter region of *c-myc* in tumor cell.

In addition, the protein protection of telomeres 1 (POT1) binds the ssDNA overhangs at the ends of chromosomes and is essential for chromosome end-protection and involved in telomere-length regulation.[28,29] hPOT1 may disrupt G-quadruplex structure in telomeric DNA and functions as a telomere maintenance element.[30] ChIP was also carried out to probe physical occupancy of POT-1 to telomeric ssDNA overhangs in the HeLa S3 cell line. As shown in Figure 1C, PCR amplification of the telomere did not show significant decrease in immunoprecipitated samples after the treatment with **1**, which indicated that the ligand could not interfere with the binding between the single-strand overhang of telomere and hPOT-1 (the raw qPCR data are also shown in Supporting Information Table S3).

Inhibition of the Elongation of Telomere by the Compound. Telomerase catalyzes the elongation of telomere, which involves complicated processes, such as the association and dissociation of catalytic enzyme. G-Quadruplex ligand may affect the event mainly through two pathways, down-regulation of *c-myc* and hTERT, or stabilization of the telomeric G-rich end to block the association of catalytic enzyme.[2] The inhibition of telomerase and interruption of its interaction with telomere G-overhang in cancer cells are suggested to disrupt telomere length maintenance and cause telomeres to erode. To investigate whether the ligand could cause the shortening of telomeres, the telomere length was determined with the telomeric restriction fragment (TRF) length assay. The results showed that 0.1 μM of **1** triggered telomere shortening for about 1.6 kb in Ramos cells, and telomere shortening was also observed after treatment with 0.05 μM of **1** (Figure 3A), while in CA46 cells, **1** could only reduce the telomere length for 0.8 kb (Figure 3B). These results

dx.doi.org/10.1021/jm200062u |*J. Med. Chem.* 2011, 54, 5671–5679

indicated that **1** could inhibit the elongation of telomere, and the telomere shortening effect might be mainly due to its direct interaction with telomerase regulated by c-Myc.

The Compound Could Induce Cell Senescence and Arrest Cell Proliferation. After 16-day treatment with **1**, the Ramos cells displayed increased proportion of flat and giant cells with phenotypic characteristics of senescence as revealed by the senescence-associated β-galactosidase (SA-β-Gal) assay method (Figure 4). This could be explained with the reason that dysfunctional telomeres could activate p53 to initiate cellular senescence or apoptosis to suppress tumorigenesis. This result indicated that the effect of **1** to induce senescence might be mainly due to the shortening of telomere length. On the other hand, the effect of **1** on CA46 cells was not obvious.

The cytotoxicity of **1** on different tumor cells was studied using MTT assay (Supporting Information Table S4). The types of tumor cells used in the present study include nasopharyngeal carcinoma, gastric cancer, hepatoma, breast carcinoma, leukemia, and lymphoma. **1** showed strong inhibitory activities on the proliferation of all tumor cells, with IC_{50} values ranging from 0.24 to 4.8 μM.

On the basis of the results of short-term proliferation assay, subcytotoxic concentrations of the ligand were used in the long term proliferation assay. The two cell lines, Ramos and CA46, were treated with **1** at indicated concentrations, with cell counts and viability determined every four days, and the incubations were finished after the growth arrest was observed. As shown in

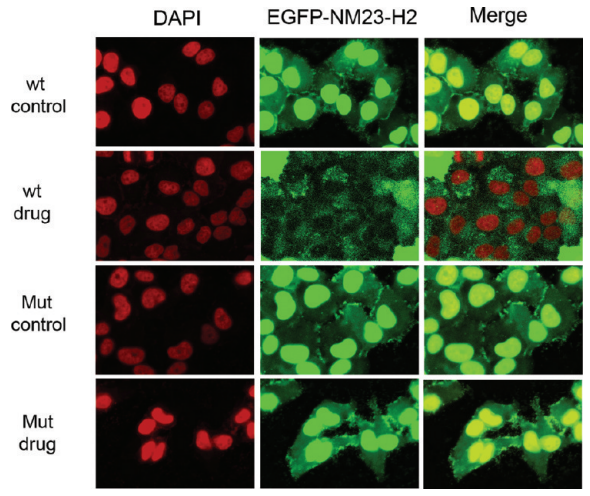

Figure 2. Confocal imaging for Hela cells. The cells were cotransfected with an EGFP-NM23-H2 fusion plasmid and a luciferase plasmid carrying the wild-type promoter region of *c-myc* (wt) or a luciferase plasmid carrying the mutant promoter region of *c-myc* (mut) and were treated with 0.1 μM **1** (drug) or 0.1% DMSO as negative control (control), respectively. After DAPI staining, the cells were imaged using a laser scanning confocal microscope. Pictures were taken with a green and red excitation filter from the same cell population and shown individually and as an overlay.

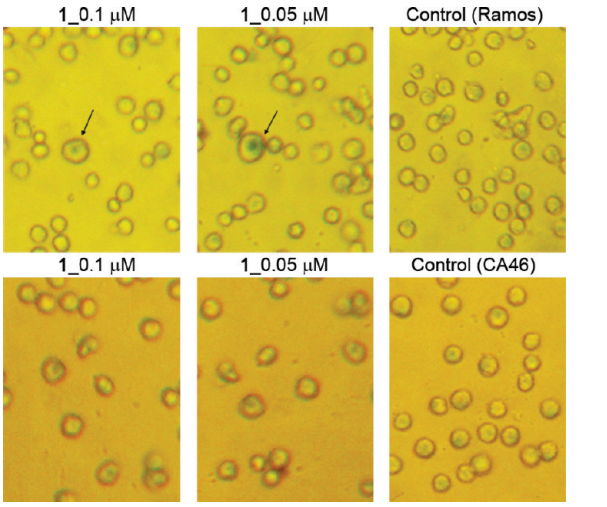

Figure 4. Expression of SA-β-Gal in Ramos and CA46 cells after continuous treatment with **1**. Ramos and CA46 cells were treated with 0.1 and 0.05 μM **1** or 0.1% DMSO continuously for 16 days. Then, the cells were fixed, stained with SA-β-Gal staining kit, and photographed. The experiment was repeated twice.

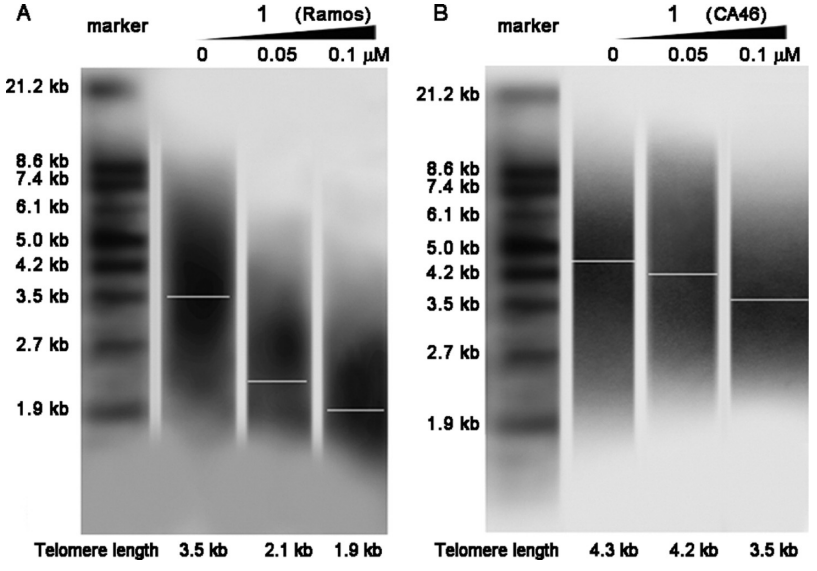

Figure 3. Effect of **1** on telomere elongation. TRF of tumor cells treated with ligands was analyzed using the *T*elo *TAGGG* telomere length assay. Ramos (A) and CA46 (B) cells were treated with **1** for 16 days.

dx.doi.org/10.1021/jm200062u |*J. Med. Chem.* 2011, 54, 5671–5679

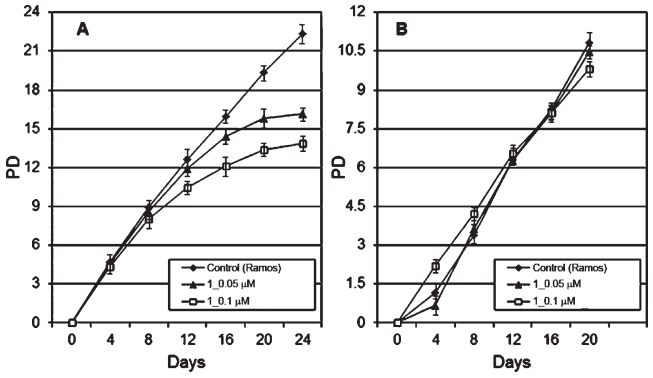

Figure 5. Long-term exposure of Ramos (A) and CA46 (B) cells to **1** at subcytotoxic concentrations. The cells were exposed to indicated concentrations of **1** or 0.1% DMSO, respectively. Every 4 days, the cells in control and drug-exposed flasks were counted and flasks reseeded with cells. Each experiment was performed three times for each point.

Figure 5, the proliferation of Ramos was inhibited by **1** (0.05 μM) after day 12 and was arrested at day 20, and the arrest activity showed concentration-dependency. For the cell line CA46 whose NHE III_1 element was removed, the inhibitory activity of **1** on cells was reduced comparing with Ramos.

On the basis of all above consistent experimental results, a hypothesis was raised for the mechanism of the effect of **1** on tumor cells. It was possible that the interaction between **1** and the G-quadruplex in the promoter of *c-myc* (mainly in the NHE III_1 element) played a key role for its antitumor activity, but its interaction with telomeric quadruplex was not significant.

■ DISCUSSION AND CONCLUSIONS

The unique structural characteristics of G-quadruplexes and their polymorphism conformations contribute to their various biological roles, which become the basis of ligand design. Meanwhile, the use of small molecular ligands as therapeutic agents targeting G-quadruplexes of oncogenes in vivo raises concerns about their selectivity and cross reactivity. The design and discovery of a good lead compound with high selectivity on G-quadruplex over duplex DNA has become possible through some modification strategies such as increasing the number of side chains,[31−33] using the side chains with the most compactable structures,[34−36] and using the unfused scaffold.[37−40] However, the design of G-quadruplex ligands with minimum cross reactivity on different G-quadruplex DNA is relatively difficult and has seldom been reported so far. Recently, it has been reported that TMPyP4 binds the parallel form of the quadruplex stronger than the antiparallel counterpart in vitro, based on UV, ITC, and SPR analysis results.[41] The two forms of quadruplex have obvious differences in their loop orientation, which might be important for molecular recognition and the selective binding of small molecules. The G-rich telomeric end and the G-rich sequence in the P1 promoter of *c-myc* are two important G-quadruplex DNAs with different conformations. The conformation of *c-myc* in solution displays a typical parallel form of G-quadruplex,[16] while the conformation of telomeric DNA in solution displays a hybrid form of G-quadruplex.[42]

The telomere maintenance is regulated with two mechanisms, including the elongation catalyzed by reactivated telomerase, and an alternative lengthening of telomere (ALT) mechanism. Telomerase is found to overexpress in the majority of tumor cells (85−90%),[43] and the unlimited proliferative potential of cancer cells depends on telomere maintenance.[44] The p53-mediated senescence mechanism is found to be in response to short telomeres that suppressed tumorigenesis.[45] In addition, *c-myc* is an important oncogene that is involved in cell proliferation, apoptosis, and senescence. The protein c-Myc has the activity on controlling the transcription level of hTERT, which is the main catalytic unit of telomerase.[46] In the present investigation, two cell lines, Ramos and CA46, were chosen for the comparative studies, and CA46 has its P1 and P2 promoter of *c-myc* removed. The hypothesis for the mechanism was raised through the analysis of all the cellular assay data together with the in vitro assay data.

The data from all the in vitro assay, including PCR stop assay, FRET-melting assay, ITC, and molecular docking, revealed that the quindoline derivative **1** had relatively stronger affinity to G-quadruplex DNA in *c-myc* promoter. Further cellular assays gave evidence that **1** exhibited its antitumor activity on tumor cells mainly through its interaction with *c-myc*. The major pathway for the effect of **1** on tumor cells might involve the following: (1) interacting with and stabilizing G-quadruplex in the promoter of *c-myc* and down-regulating its transcription and expression, (2) inhibiting the expression of *c-myc*'s downstream target hTERT, (3) down-regulation of hTERT inducing the inhibition of telomerase activity, (4) blocking the binding of the transcription regulation protein NM23-H2 to the promoter region of *c-myc*, (5) inhibition of the telomere elongation, and finally inducing lymphomas cells senescence and arresting cell proliferation. Specially, although the promoter region of hTERT could also form a G-quadruplex structure,[47] the direct interaction between **1** and hTERT seemed not to play a key role in the whole pathway.

The wide existence of G-rich sequence in the regulatory region of human genome makes it difficult to find a G-quadruplex ligand targeting single gene in vivo. Even though, based on the polymorphism of G-quadruplexes, it is realistic and possible to discover a ligand with minimum cross reactivity. The results in the present study might shed light on the design and discovery of new ligands with higher quadruplex selectivity and antitumor activity but with minimum cross reactivity in tumor cells.

■ EXPERIMENTAL SECTION

Materials and Synthesis. All Chemicals were obtained from commercial sources unless otherwise specified. Synthesis and characterization of *N*′-(10*H*-indolo[3,2-*b*]-quinolin-11-yl)-*N*,*N*-dimethyl-ethane-1,2-diamine (**1**) was performed as previously reported.[22] The compound was identified with NMR, high-resolution mass spectra, and elemental analysis, which also confirmed that the purity of the compound was more than 95% .

All oligomers/primers were purchased from Invitrogen (China). Stock solutions of both ligands (10 mM) were prepared using DMSO and stored at −80 °C. Their dilutions to working concentrations were carried out with relevant buffer immediately prior to usage. The primary antibodies and horseradish peroxidase-conjugated secondary antibody were purchased from Chemicon International, Inc., USA. All tumor cell lines were obtained from the American Type Culture Collection (ATCC, Rockville, MD). The cell culture was maintained in a RPMI-1640 or DMEM medium supplemented with 10% fetal bovine serum, 100 U/mL penicillin, and 100 μg/mL streptomycin in 25 cm^2 culture flasks at 37 °C under humidified atmosphere with 5% CO_2.

FRET Assay. FRET assay was carried out on a real-time PCR apparatus (Roche LightCycler 2). The labeled oligonucleotides F21T (5′-*FAM*-d(GGGTTAGGGTTAGGGTTAGGG)-*TAMRA*-3′) and Pu27 (5′-*FAM*-d(TGGGGAGGGTGGGGAGGGTGGGGAAGG)-*TAMRA*-3′) as the FRET probes were diluted from the stock solution to the required concentration (400 nM) in Tris-HCl buffer (10 mM, pH 7.2) containing KCl. The mixture of 10 μL of native F21T (400 nM) or dual-Pu27 and 10 μL of compound solution at 2 μM was first annealed by heating at 90 °C for 5 min, followed with cooling to room temperature in a thermocycler. The resulting 20 μL solutions were added into LightCycler capillaries, and the measurements were made in duplicate on a Roche LightCycler 2 with excitation at 470 nm and detection at 530 nm. Fluorescence readings were taken at intervals of 1 °C over the range of 37−99 °C, with a constant temperature maintained for 30 s prior to each reading to ensure a stable value. Final analysis of the data was carried out using Origin 6.0 (OriginLab Corp.).

PCR Stop Assay. The reaction was carried out in 1× PCR buffer, containing 2 μmol of a pair of oligomers: Pu27 (5′-TGGGGAGGGTGGGGAGGGTGGGGAAGG-3′) or HTG 21 (5′-GGGTTAGGGTTAGGGTTAGG-3′), and its corresponding complementary sequence Pu27rev (5′-ATCGATCTCTTCTCGTCCTTCCCCA-3′) or HTG21rev (5′-ATCGCTTCTCGTCCCTAA CC-3′), 0.16 mM dNTP, 2.5 U *Taq* polymerase, and a certain concentration of the compound. The reaction mixture was incubated in a Mastercycler Personal (Eppendorf) with the following cycling conditions: 94 °C for 3 min, followed with 10 cycles of 94 °C for 30 s, 58 °C for 30 s, and 72 °C for 30 s. The amplified product was resolved with 15% nondenaturing polyacrylamide gel in 1× TBE followed with silver staining.

ITC Measurement. ITC measurements were carried out in a VP-ITC titration calorimeter (MicroCal, Northampton, MA). Before loading, the solutions were thoroughly degassed. The reference cell was filled with the degassed buffer. The quadruplex (8.75 μM) was kept in the sample cell, and **1** (400 μM, 300 μL) in the same buffer was added sequentially in 10 μL aliquots (for a total of 30 injections, 20 s duration each) at 4 min intervals at 25 °C. In control experiments, the heats of dilution were determined in parallel experiments by injecting **1** solution of the same concentration in the same buffer. The heats of dilution were subtracted from the corresponding binding experiments prior to curve fitting. The thermograms (integrated heat/injection data) obtained in ITC experiments were fit with proper model in Origin 6.0.

Molecular Modeling. The NMR structure of telomeric G-quadruplex (PDB 2HY9)[48] and the *c-myc* G-quadruplex structure built by Tian-Miao Ou et al.[13] were used as an initial models. Ligand structures were constructed within SYBYL7.3 (Tripos Inc., St Louis, MO, USA). Docking studies were performed using the AUTODOCK 4.0 program.[49] The dimensions of the active site box were chosen to be large enough to encompass the entire DNA molecule. Docking calculations were carried out using the Lamarckian genetic algorithm (LGA). The most possible conformation of the ligand was chosen based on the consideration of its lowest final docked energy and its optimal binding arrangement with the G-tetrads.

MD simulations were performed using the sander module of the AMBER 10.0 program suite.[50] The complexes were solvated in a octahedral box of TIP3P water molecules with 10 Å solvent layers. The potassium counterions were added to neutralize the systems. Periodic boundary conditions and the particle mesh Ewald algorithm were used. The hydrogen bonds were constrained using SHAKE. The solvated structures were subjected to initial minimization to equilibrate the solvent and counter cations. The system was then heated from 0 to 300 K in a 100 ps simulation, followed with a 100 ps simulation to equilibrate the density of the system. Afterward, constant pressure MD simulation of 2 ns was then performed in an NPT ensemble at 1 atm and 300 K. The MM/PBSA method[50] was used to calculate the binding free energy. All the waters and counterions were stripped off except the K^+ present within the electronegatively charged central channel. The set of 200 snapshots from the last MD trajectories were collected to calculate the binding free energies.

Cellular Uptake Experiments. After 4 days of treatment with or without **1**, Ramos and CA46 lymphoma cells were harvested and washed with PBS (pH 7.4) for three times and 1×10^6 cells were reresuspended in the extraction buffer (60% ethanol and 0.3 M HCl) and lysed using a SCIENTZ-II D sonicator (SCIENTZ). Then the lysate centrifuged at 18000*g* at 4 °C for 10 min, and the supernatant was diluted by extraction buffer to 3 mL. Fluorescence measurements were carried out on a Perkin-Elmer LS55 fluorescence spectrometer. The excitation and emission slits were both 10 nm. Excitation was set at 337 nm. Standard curve was generated from the emission fluorescence intensity of a series of dilutions of ligand with the concentrations from 0.003125 to 0.2 μM at 448 nm. The uptaking concentration of ligand was calculated from the standard curve. A buffer blank or a cell lysate blank without ligand was subtracted for all samples.

Long-Term Cell Culture Experiments. Long-term proliferation experiments were carried out using the Ramos and CA46 lymphoma cell line. Cells (1.0×10^5) were grown in 10 cm Petri dishes and exposed to a subcytotoxic concentration of a ligand or an equivalent volume of 0.1% DMSO every 4 days. The cells in control and drug-exposed dishes were counted, and the dishes reseeded with 1.0×10^5 cells. The remaining cells were collected and used for measurements described below. This process was continued for 16 days or 20 days.

Real-Time RT-PCR. After incubation, the cells were washed with PBS (pH 7.4) and the cell pellets were lysed in TRIzol solution. Total RNA was extracted according to the protocol supplied by Takara Company and eluted in distilled, deionized water with 0.1% diethyl pyrocarbonate (DEPC) to a final volume of 50 μL. RNA was quantitated spectrophotometrically. Total RNA was used as a template for reverse transcription using the following protocol: each 20 μL reaction contained 1× M-MLV buffer, 500 μM dNTP, 100 pmol oligo dT18 primer, 100 units of M-MLV reverse transcriptase, DEPC-H_2O, and 1 μg of total RNA. The mixtures was incubated at 42 °C for 60 min for reverse transcription, and then at 92 °C for 10 min.

Real-time PCR was performed on a real-time PCR apparatus (Roche LightCycler 2) by using SYBR Premix Ex *Taq* (Takara), according to the manufacturer's protocol. The total volume of 20 μL real-time RT-PCR reaction mixtures contained 10 μL of SYBR Premix Ex Taq, 0.4 μM each of forward and reverse primers, and 1 μL of cDNA and nuclease-free water. The program used for all genes consisted of a denaturing cycle of 3 min at 95 °C, 45 cycles of PCR (95 °C for 20 s, 58 °C for 30 s, and 68 °C for 30 s), a melting cycle consisted of 95 °C for 15 s, 65 °C for 15 s, and a step cycle starting at 65 °C with a 0.2 °C/s transition rate to 95 °C. The specificity of the real-time RT-PCR product was confirmed by melting curve analysis. The PCR product sizes were confirmed with agarose gel electrophoresis and ethidium bromide staining. Three replications were performed, and then *c-myc* and *hTERT* mRNA levels were normalized to *GAPDH* mRNA level of each sample. Results of real-time PCR were analyzed using $2^{-\Delta CT}$ method to compare the transcriptional levels of *c-myc* and *hTERT* genes in each sample relative to a control without drug treatment.

The primers used in the real-time RT-PCR were: *c-myc* A (5′-TGGTGCTCCATGAGGAGACA-3′), *c-myc* S (5′-GTGGCACCTCTTGAGGACCT-3′), hTERT A (5′-GGATGAAGC GGAGTCTGGA-3′), hTERT S (5′-CGGAAGAGTGTCTGGA GCAA-3′), GAPDH A (5′-GATGACATCAAGAAGGTGG-TG-3′), and GAPDH S (5′-GCTGTA GCCAAATTCGTTGTC-3′).

Western Blot. Cells harvested from each well of the culture plates were lysed in 150 μL of extraction buffer consisted of 100 μL of solution A (50 mM glucose, 25 mM Tris-HCl, pH 8, 10 mM EDTA, 1 mM PMSF) and 50 μL of solution B (50 mM Tris-HCl, pH 6.8, 6 M urea, 6% 2-mercaptoethanol, 3% SDS, 0.003% bromophenol blue). The

suspension was centrifuged at 10000 rpm at 4 °C for 5 min, and the supernatant (10 μL for each sample) was loaded onto 10% polyacrylamide gel and then transferred to a microporous polyvinylidene difluoride (PVDF) membrane. Western blotting was performed using anti-c-Myc (Santa Cruze Biotechnology), anti-hTERT (Chemicon), or anti-β-actin (Chemicon) antibody, and horseradish peroxidase-conjugated antimouse or antirabbit secondary antibody. Protein bands were visualized using chemiluminescence substrate.

Ch-IP. Chromatin immunoprecipitation (ChIP) was performed using Magna ChIPTM kit (Millipore) following manufacturer's protocol. After 4 days of treatment with or without ligand, antibody against NM23-H2 (Santa Cruz Biotechnology, SC-100400) or POT-1 (Santa Cruz Biotechnology, SC-33789) were used to immunoprecipitate chromatin in HeLa cells. Rabbit IgG was used for mock immunoprecipitation. Briefly, cells were fixed with 1% formaldehyde for 10 min and then lysed. Chromatin was sheared to an average size of 0.5 kb using a SCIENTZ-II D sonicator (SCIENTZ), and 1% of lysate was removed as input. ChIP was performed overnight at 4 °C, and immune complexes were collected using protein A magnetic beads provided by the kit. After extensive washing, the DNA was extracted from immunoprecipitated chromatin. Immunoprecipitated DNA samples were amplified using quantitative PCR, as described before, to show POT-1 or NM23-H2 occupancy of *c-myc* promoter or telomeric single-stranded end and negative control. The primer sequences used here were: *c-myc* 1: CTACGGAGGAGCAGCA GAGAAAG, *c-myc* 2: GTGGGGAGGGTGGGGAAGGT. *tel* 1: GGTTT-TTGAGGGTGAGGG TGAGGGTGAGGGTGAGGGT, *tel* 2: TCCCGACTATCCCTATCCCTATCCCTATCCCTAT CCCTA.

Plasmid Construction. The EGFP-NM23-H2 fusion plasmid was constructed by inserting human NM23-H2 cDNA into pEGFP-N3 (invitrogen) using *Eco*RI and *Bam*HI. The luciferase plasmids containing wild-type or mutant promoter region in *c-myc* were gifts from Professor Laurence H. Hurley (University of Arizona, USA).[26]

Transfection and Confocal Imaging. Cells (8.0×10^5) were grown in 3 cm Petri dishes, and after 24 h, DNA transfections were performed as follows: first, 2.0 μg c-myc plasmid or mut-c-myc plasmid and 2.0 μg EGFP-NM23-H2 were cotranfected into cells using Lipo2000 (invitrogen). Then, **1** was added into medium after 6 h of transfection. After another 24 h of drug treatment, the cells were stained by DAPI and imaged using a Zeiss LSM 710 laser scanning confocal microscope.

Telomere Length Assay. Cells were incubated with the ligand for 16 days. To measure the telomere length, genomic DNA was digested with Hinf1/Rsa1 restriction enzymes. The digested DNA fragments were separated on 0.8% agarose gel, transferred to a nylon membrane, and the transferred DNA fixed on the wet blotting membrane by baking the membrane at 120 °C for 20 min. The membrane was hybridized with a DIG-labeled hybridization probe for telomeric repeats and incubated with anti-DIG-alkaline phosphatase. TRF was performed with chemiluminescence detection.

SA-β-Gal Assay. After the long-term incubation, the growth medium was aspirated and the cells were fixed in 2% formaldehyde/0.2% glutaraldehyde for 15 min at room temperature. The fixing solution was removed, and the cells were gently washed twice with PBS and then stained using the β-Gal staining solution containing 1 mg/mL of 5-bromo-4-chloro-3-indolyl-β-D-galactoside, followed with incubation overnight at 37 °C. The staining solution was removed, and the cells were washed three times with PBS. The cells were viewed under an optical microscope and photographed.

■ ASSOCIATED CONTENT

Supporting Information. The docking results of **1** with G-quadruplex containing DNA; all the raw data from FRET-melting, ITC, and PCR stop assay, real-time PCR; the cellular uptake experiment results; the raw data from real-time PCR in transcription level detection and ChIP; the IC_{50} values of **1** on different tumor cells from MTT assay. This material is available free of charge via the Internet at http://pubs.acs.org.

■ AUTHOR INFORMATION

Corresponding Author

*For Z.-S.H.: phone, 8620-39943056; fax, 8620-39943056; E-mail, ceshzs@mail.sysu.edu.cn. For L.-Q.G.: phone, 8620-39943055; fax, 8620-39943056; E-mail, cesglq@mail.sysu.edu.cn.

Author Contributions

§These authors contributed equally to this paper.

■ ACKNOWLEDGMENT

We thank the Natural Science Foundation of China (grants U0832005 for L.-Q. Gu, 90813011 and 20772159 for Z.-S. Huang, 30801436 for T.-M. Ou), the International S&T Cooperation Program of China (grant 2010DFA34630 for L.-Q. Gu), the Ministry of Education of the People's Republic of China (grant 200805581163 for T.-M. Ou), the Fundamental Research Funds for the Central Universities (T.-M. Ou), the Guangdong Natural Science Foundation (grant 8451008901000214 for T.-M. Ou), and the Science Foundation of Guangzhou (2009A1-E011-6 for Z.-S. Huang). We also thank Professor Laurence H. Hurley (University of Arizona) for the advice on this article and the plasmid gifts.

■ ABBREVIATIONS USED

G guanine; hTERT human telomerase reverse transcriptase; NMR nuclear magnetic resonance; DMSO dimethyl sulfoxide; FRET fluorescence resonance energy transfer; ITC isothermal titration calorimetry; MD molecular docking; qRT-PCR quantitative reverse transcription PCR; Ch-IP chromatin immunoprecipitation; POT-1 protection of telomerase 1; TRF telomeric restriction fragment; SA-β-Gal senescence-associated β-galactosidase; IC_{50} concentration for 50% inhibition; NHE III1 nuclease hypersensitive element III1; MTT methylthiazolyldiphenyl-tetrazolium bromide; SPR surface plasmon resonance

■ REFERENCES

(1) Ou, T.-M.; Lu, Y.-J.; Tan, J.-H.; Huang, Z.-S.; Wong, K.-Y.; Gu, L.-Q. G-quadruplexes: targets in anticancer drug design. *ChemMedChem* **2008**, *3*, 690–713.

(2) De Cian, A.; Lacroix, L.; Douarre, C.; Temime-Smaali, N.; Trentesaux, C.; Riou, J.-F.; Mergny, J.-L. Targeting telomeres and telomerase. *Biochimie* **2008**, *90*, 131–155.

(3) Neidle, S.; Parkinson, G. N.; Quadruplex, D. N. A. crystal structures and drug design. *Biochimie* **2008**, *90*, 1184–1196.

(4) Balasubramanian, S.; Hurley, L. H.; Neidle, S. Targeting G-quadruplexes in gene promoters: a novel anticancer strategy? *Nature Rev. Drug Discovery* **2011**, *10*, 261–275.

(5) Izbicka, E.; Wheelhouse, R. T.; Raymond, E.; Davidson, K. K.; Lawrence, R. A.; Sun, D.; Windle, B. E.; Hurley, L. H.; Von Hoff, D. D. Effects of cationic porphyrins as G-quadruplex interactive agents in human tumor cells. *Cancer Res.* **1999**, *59*, 639–644.

(6) Gowan, S. M.; Heald, R.; Stevens, M. F. G.; Kelland, L. R. Potent inhibition of telomerase by small-molecule pentacyclic acridines capable of interacting with G-quadruplexes. *Mol. Pharmacol.* **2001**, *60*, 981–988.

(7) Gowan, S. M.; Harrison, J. R.; Patterson, L.; Valenti, M.; Read, M. A.; Neidle, S.; Kelland, L. R. A G-quadruplex-interactive potent small-molecule inhibitor of telomerase exhibiting in vitro and in vivo antitumor activity. *Mol. Pharmacol.* **2002**, *61*, 1154–1162.

(8) Zhou, W. J.; Deng, R.; Zhang, X. Y.; Feng, G. K.; Gu, L. Q.; Zhu, X. F. G-Quadruplex ligand SYUIQ-5 induces autophagy by telomere damage and TRF2 delocalization in cancer cells. *Mol. Cancer Ther.* **2009**, *8*, 3203–3213.

(9) Riou, J. F.; Guittat, L.; Mailliet, P.; Laoui, A.; Renou, E.; Petitgenet, O.; Megnin-Chanet, F.; Helene, C.; Mergny, J. L. Cell senescence and telomere shortening induced by a new series of specific G-quadruplex DNA ligands. *Proc. Natl. Acad. Sci. U.S.A.* **2002**, *99*, 2672–2677.

(10) Tauchi, T.; Shin-ya, K.; Sashida, G.; Sumi, M.; Nakajima, A.; Shimamoto, T.; Ohyashiki, J. H.; Ohyashiki, K. Activity of a novel G-quadruplex-interactive telomerase inhibitor, telomestatin (SOT-095), against human leukemia cells: involvement of ATM-dependent DNA damage response pathways. *Oncogene* **2003**, *22*, 5338–5347.

(11) Pennarun, G.; Granotier, C.; Gauthier, L. R.; Gomez, D.; Hoffschir, F.; Mandine, E.; Riou, J.-F.; Mergny, J.-L.; Mailliet, P.; Boussin, F. D. Apoptosis related to telomere instability and cell cycle alterations in human glioma cells treated by new highly selective G-quadruplex ligands. *Oncogene* **2005**, *24*, 2917–2928.

(12) Incles, C. M.; Schultes, C. M.; Kempski, H.; Koehler, H.; Kelland, L. R.; Neidle, S. A G-quadruplex telomere targeting agent produces p16-associated senescence and chromosomal fusions in human prostate cancer cells. *Mol. Cancer Ther.* **2004**, *3*, 1201–1206.

(13) Ou, T.-M.; Lu, Y.-J.; Zhang, C.; Huang, Z.-S.; Wang, X.-D.; Tan, J.-H.; Chen, Y.; Ma, D.-L.; Wong, K.-Y.; Tang, J. C.-O.; Chan, A. S.-C.; Gu, L.-Q. Stabilization of G-quadruplex DNA and down-regulation of oncogene c-myc by quindoline derivatives. *J. Med. Chem.* **2007**, *50*, 1465–1474.

(14) Sun, D.; Liu, W.-J.; Guo, K.; Rusche, J. J.; Ebbinghaus, S.; Gokhale, V.; Hurley, L. H. The proximal promoter region of the human vascular endothelial growth factor gene has a G-quadruplex structure that can be targeted by G-quadruplex-interactive agents. *Mol. Cancer Ther.* **2008**, *7*, 880–889.

(15) Seenisamy, J.; Bashyam, S.; Gokhale, V.; Vankayalapati, H.; Sun, D.; Siddiqui-Jain, A.; Streiner, N.; Shinya, K.; White, E.; Wilson, W. D.; Hurley, L. H. Design and Synthesis of an Expanded Porphyrin That Has Selectivity for the c-MYC G-Quadruplex Structure. *J. Am. Chem. Soc.* **2005**, *127*, 2944–2959.

(16) Seenisamy, J.; Rezler, E. M.; Powell, T. J.; Tye, D.; Gokhale, V.; Joshi, C. S.; Siddiqui-Jain, A.; Hurley, L. H. The dynamic character of the G-quadruplex element in the c-MYC promoter and modification by TMPyP4. *J. Am. Chem. Soc.* **2004**, *126*, 8702–8709.

(17) Dang, C. V. c-Myc target genes involved in cell growth, apoptosis, and metabolism. *Mol. Cell. Biol.* **1999**, *19*, 1–11.

(18) Flores, I.; Evan, G.; Blasco, M. A. Genetic analysis of myc and telomerase interactions in vivo. *Mol. Cell. Biol.* **2006**, *26*, 6130–6138.

(19) Sampedro Camarena, F.; Cano Serral, G.; Sampedro Santalo, F. Telomerase and telomere dynamics in ageing and cancer: current status and future directions. *Clin. Transl. Oncol.* **2007**, *9*, 145–154.

(20) Zhou, J. M.; Zhu, X. F.; Lu, Y. J.; Deng, R.; Huang, Z. S.; Mei, Y. P.; Wang, Y.; Huang, W. L.; Liu, Z. C.; Gu, L. Q.; Zeng, Y. X. Senescence and telomere shortening induced by novel potent G-quadruplex interactive agents, quindoline derivatives, in human cancer cell lines. *Oncogene* **2006**, *25*, 503–511.

(21) Zhou, W. J.; Deng, R.; Zhang, X. Y.; Feng, G. K.; Gu, L. Q.; Zhu, X. F. G-quadruplex ligand SYUIQ-5 induces autophagy by telomere damage and TRF2 delocalization in cancer cells. *Mol. Cancer Ther.* **2009**, *8*, 3203–3213.

(22) Zhou, J.-L.; Lu, Y.-J.; Ou, T.-M.; Zhou, J.-M.; Huang, Z.-S.; Zhu, X.-F.; Du, C.-J.; Bu, X.-Z.; Ma, L.; Gu, L.-Q.; Li, Y.-M.; Chan, A. S.-C. Synthesis and Evaluation of Quindoline Derivatives as G-Quadruplex Inducing and Stabilizing Ligands and Potential Inhibitors of Telomerase. *J. Med. Chem.* **2005**, *48*, 7315–7321.

(23) Simonsson, T.; Henriksson, M. c-myc Suppression in Burkitt's Lymphoma Cells. *Biochem. Biophy. Res. Commun.* **2002**, *290*, 11–15.

(24) Postel, E. H.; Berberich, S. J.; Flint, S. J.; Ferrone, C. A. Human c-myc transcription factor PuF identified as nm23−2 nucleoside diphosphate kinase, a candidate suppressor of tumor metastasis. *Science* **1993**, *261*, 478–480.

(25) Facchini, L. M.; Penn, L. Z. The molecular role of Myc in growth and transformation: recent discoveries lead to new insights. *FASEB J.* **1998**, *12*, 633–651.

(26) Dexheimer, T. S.; Carey, S. S.; Zuohe, S.; Gokhale, V. M.; Hu, X.; Murata, L. B.; Maes, E. M.; Weichsel, A.; Sun, D.; Meuillet, E. J.; Montfort, W. R.; Hurley, L. H. NM23-H2 may play an indirect role in transcriptional activation of c-myc gene expression but does not cleave the nuclease hypersensitive element III1. *Mol. Cancer Ther.* **2009**, *8*, 1363–1377.

(27) Thakur, R. K.; Kumar, P.; Halder, K.; Verma, A.; Kar, A.; Parent, J.-L.; Basundra, R.; Kumar, A.; Chowdhury, S. Metastases suppressor NM23-H2 interaction with G-quadruplex DNA within c-MYC promoter nuclease hypersensitive element induces c-MYC expression. *Nucleic Acids Res.* **2009**, *37*, 172–183.

(28) Lei, M.; Zaug, A. J.; Podell, E. R.; Cech, T. R. Switching human telomerase on and off with hPOT1 protein in vitro. *J. Biol. Chem.* **2005**, *280*, 20449–20456.

(29) Lei, M.; Podell, E. R.; Baumann, P.; Cech, T. R. DNA self-recognition in the structure of Pot1 bound to telomeric single-stranded DNA. *Nature* **2003**, *426*, 198–203.

(30) Zaug, A. J.; Podell, E. R.; Cech, T. R. Human POT1 disrupts telomeric G-quadruplexes allowing telomerase extension in vitro. *Proc. Natl. Acad. Sci. U.S.A.* **2005**, *102*, 10864–10869.

(31) Cuenca, F.; Greciano, O.; Gunaratnam, M.; Haider, S.; Munnur, D.; Nanjunda, R.; Wilson, W. D.; Neidle, S. Tri- and tetra-substituted naphthalene diimides as potent G-quadruplex ligands. *Bioorg. Med. Chem. Lett.* **2008**, *18*, 1668–1673.

(32) Harrison, R. J.; Cuesta, J.; Chessari, G.; Read, M. A.; Basra, S. K.; Reszka, A. P.; Morrell, J.; Gowan, S. M.; Incles, C. M.; Tanious, F. A.; Wilson, W. D.; Kelland, L. R.; Neidle, S. Trisubstituted Acridine Derivatives as Potent and Selective Telomerase Inhibitors. *J. Med. Chem.* **2003**, *46*, 4463–4476.

(33) Rangan, A.; Fedoroff, O. Y.; Hurley, L. H. Induction of duplex to G-quadruplex transition in the c-myc promoter region by a small molecule. *J. Biol. Chem.* **2001**, *276*, 4640–4646.

(34) Zagotto, G.; Sissi, C.; Lucatello, L.; Pivetta, C.; Cadamuro, S. A.; Fox, K. R.; Neidle, S.; Palumbo, M. Aminoacyl-anthraquinone conjugates as telomerase inhibitors: synthesis, biophysical and biological evaluation. *J. Med. Chem.* **2008**, *51*, 5566–5574.

(35) Pivetta, C.; Lucatello, L.; Krapcho, A. P.; Gatto, B.; Palumbo, M.; Sissi, C. Perylene side chains modulate G-quadruplex conformation in biologically relevant DNA sequences. *Bioorg. Med. Chem.* **2008**, *16*, 9331–9339.

(36) Rossetti, L.; Franceschin, M.; Schirripa, S.; Bianco, A.; Ortaggi, G.; Savino, M. Selective interactions of perylene derivatives having different side chains with inter- and intramolecular G-quadruplex DNA structures. A correlation with telomerase inhibition. *Bioorg. Med. Chem. Lett.* **2005**, *15*, 413–420.

(37) Dash, J.; Shirude, P. S.; Balasubramanian, S. G-Quadruplex recognition by bis-indole carboxamides. *Chem. Commun.* **2008**, 3055–3057.

(38) Moorhouse, A. D.; Santos, A. M.; Gunaratnam, M.; Moore, M.; Neidle, S.; Moses, J. E. Stabilization of G-Quadruplex DNA by Highly Selective Ligands via Click Chemistry. *J. Am. Chem. Soc.* **2006**, *128*, 15972–15973.

(39) Wheelhouse, R. T.; Jennings, S. A.; Phillips, V. A.; Pletsas, D.; Murphy, P. M.; Garbett, N. C.; Chaires, J. B.; Jenkins, T. C. Design, Synthesis, and Evaluation of Novel Biarylpyrimidines: A New Class of Ligand for Unusual Nucleic Acid Structures. *J. Med. Chem.* **2006**, *49*, 5187–5198.

(40) Waller, Z. A. E.; Shirude, P. S.; Rodriguez, R.; Balasubramanian, S. Triarylpyridines: a versatile small molecule scaffold for G-quadruplex recognition. *Chem. Commun.* **2008**, 1467–1469.

(41) Arora, A.; Maiti, S. Effect of loop orientation on quadruplex-TMPyP4 interaction. *J. Phys. Chem. B* **2008**, *112*, 8151–8159.
(42) Luu, K. N.; Phan, A. T.; Kuryavyi, V.; Lacroix, L.; Patel, D. J. Structure of the Human Telomere in K^+ Solution: An Intramolecular (3 + 1) G-Quadruplex Scaffold. *J. Am. Chem. Soc.* **2006**, *128*, 9963–9970.
(43) Kim, N. W.; Piatyszek, M. A.; Prowse, K. R.; Harley, C. B.; West, M. D.; Ho, P. L. C.; Coviello, G. M.; Wright, W. E.; Weinrich, S. L.; Shay, J. W. Specific association of human telomerase activity with immortal cells and cancer. *Science* **1994**, *266*, 2011–2015.
(44) Hanahan, D.; Weinberg, R. A. The hallmarks of cancer. *Cell* **2000**, *100*, 57–70.
(45) Feldser, D. M.; Greider, C. W. Short telomeres limit tumor progression in vivo by inducing senescence. *Cancer Cell* **2007**, *11*, 461–469.
(46) Cerni, C. Telomeres, telomerase, and myc. An update. *Mutat. Res.* **2000**, *462*, 31–47.
(47) Palumbo, S. L.; Ebbinghaus, S. W.; Hurley, L. H. Formation of a unique end-to-end stacked pair of G-quadruplexes in the hTERT core promoter with implications for inhibition of telomerase by G-quadruplex-interactive ligands. *J. Am. Chem. Soc.* **2009**, *131*, 10878–10891.
(48) Dai, J.; Punchihewa, C.; Ambrus, A.; Chen, D.; Jones, R. A.; Yang, D. Structure of the intramolecular human telomeric G-quadruplex in potassium solution: a novel adenine triple formation. *Nucleic Acids Res.* **2007**, *35*, 2440–2450.
(49) Morris, G. M.; Goodsell, D. S.; Halliday, R. S.; Huey, R.; Hart, W. E.; Belew, R. K.; Olson, A. J. Automated docking using a Lamarckian genetic algorithm and an empirical binding free energy function. *J. Comput. Chem.* **1998**, *19*, 1639–1662.
(50) Kollman, P. A.; Massova, I.; Reyes, C.; Kuhn, B.; Huo, S. H.; Chong, L.; Lee, M.; Lee, T. Calculating structures and free energies of complex molecules: combining molecular mechanics and continuum models. *Acc. Chem. Res.* **2000**, *33*, 889–897.